Continuum Model for Lattice Deformation in Twisted Bilayer Graphene

Itgel Ganbold 18407654

Supervisor: *Nuala Caffrey*

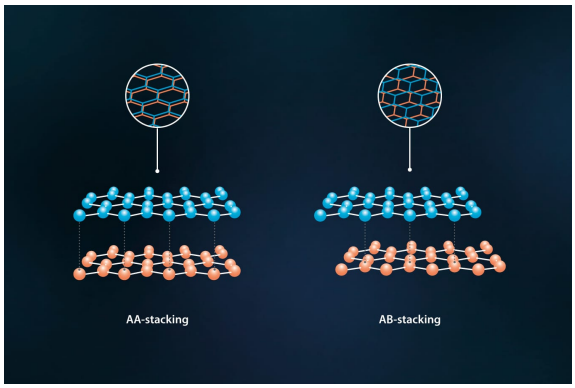

This thesis is submitted to University College Dublin in partial fulfilment of the requirements for the degree of BSc in Theoretical Physics

UCD School of Physics

April 18, 2022

Contents

List of Figures

List of Acronyms

BCS - Bardeen-Cooper-Schrieffer
BG - Bilayer graphene
DFT - Discrete Fourier Transform
HTS - High temperature superconductor
tBG - Twisted bilayer graphene

Preface

Acknowledgement

The completion of this thesis would not have been possible without the support and participation of numerous individuals. In particular, I would like to express my deep gratitude to my supervisor Dr. Nuala Caffrey for her endless support and understanding spirit throughout the year. I would also like to express my great appreciation to the staff and lecturers of the School of Physics for their expert guidance and teaching throughout my undergraduate years.

Declaration of Authorship

I declare that all material in this assessment is my own work except where there is clear acknowledgement and appropriate reference to the work of others.

Abstract

A small twist angle between two graphene sheets has yielded some surprising results in recent times. Theoretical predictions of the existence of *magic angles* were proven correct. At these twist angles, the bilayer graphene becomes superconducting. However, there was a small disagreement between theoretical predictions of the value of these angles and recently measured experimental results. In this report, we model the twisted-bilayer graphene using the Continuum model approach, where the system is treated as two continuous sheets. Calculations that account for individual atoms were shown to be intractable. We look at how this twisting of periodic structures, such as graphene produces a hexagonal moiré pattern. Our model aims to show how the forces between the layers and the forces within the layers distort the moiré pattern. This flexibility of graphene accounts for the disagreement between theory and experiment. Our model is developed ground-up from a simple 1D model to a more complex 2D model. The equations it produces were solved self-consistently using Python 3.8 simulations. We restricted our view to a small angle rotation of 1.1° as this is the value of the first *magic angle* for graphene. Further work is required to solve the equations obtained in our 2D model.

1 Introduction

Graphene is a single layer material that consists of carbon atoms arranged in a hexagonal honeycomb lattice structure. Scientists have closely studied the electronic properties of graphene since its discovery and synthesis in 2004 (Novoselov et al. 2004). A recent development on this front has been the topic of twisted bilayer graphene (tBG); a double-layered structure that scientists can twist to a precision of 0.01° thanks to its weak interlayer coupling (Cao et al. 2016 and Kim et al. 2016). Moreover, the material exhibits remarkable properties near particular twist angles, including superconductivity, as the electronic bands become highly flat (Hung Nguyen et al. 2021). While this has attracted a great deal of attention, it is important to note that this superconductivity property is currently impossible at high temperatures. These twist angles are called "*magic angles*" and the first of these *magic angles* is around 1.10° (Jarillo-Herrero, P. et al. 2018)

Another aspect of tBG is the emergent property of the moiré pattern and its role in the electronic property of bilayer graphene (BG) (He et al. 2021). A moiré pattern is an angle-dependent sizeable quasiperiodic structure that forms when two periodic layers are stacked with some relative twist angle. The electronic structures of moiré superlattices were first formulated in detail by the moiré band theory (Bistritzer and MacDonald 2011). The size of a moiré superlattice corresponds to the relative layer twist angle and thus the distances between corresponding atoms of each layer in different areas of the moiré pattern (Green and Weigle 1948). The regions where the atoms lie close to or directly above each other is called AA stacking. An AB stacking is when the corresponding atoms are far apart, and their relative distances are large. It is well known that the energy configuration of AB stacking is more favourable than AA stacking as naturally occurring graphite shows only AB stacked graphene (Pierre, 2000). The main difficulty with trying to solve for the electronic structure of a moiré pattern is that for small angles, such as in the first *magic angle*, the moiré superlattice is enormous. For a rotation of only 4.41° the moiré unit cell contains 676 atoms as shown in Figure 1. For a rotation of 1.1° a unit cell would have over ten thousand atoms. This makes the computations not tractable when accounting for each atom within the moiré unit cell and so physicists have turned to a continuum model for convenience (Lopes dos Santos, Peres, & Castro Neto

2012).

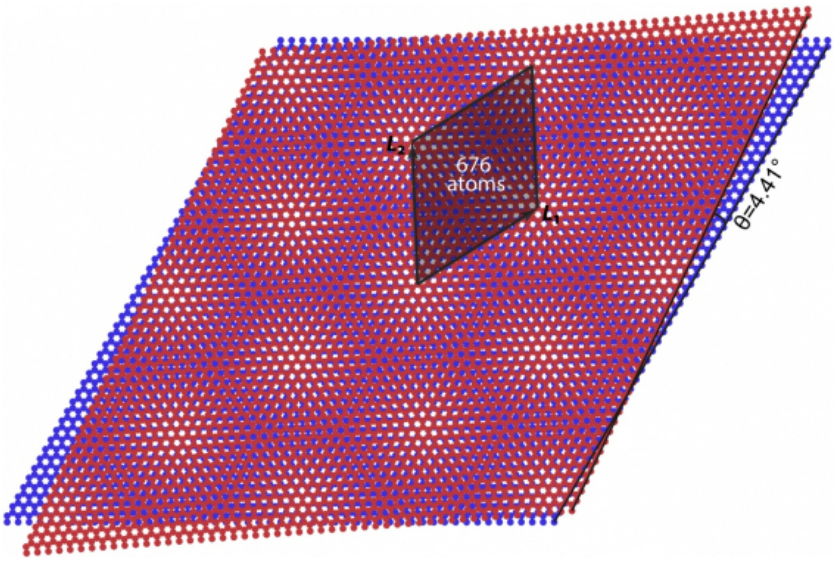

Figure 1: Moiré unit cell at a rotation angle of 4.41° contains 676 atoms.(Chen et al. 2018)

When left to its own devices and allowed to relax, the moiré pattern changes and shifts to minimize its energy. This means that the carbon atoms shift and lose their perfect honeycomb structure. The AB (incommensurate) regions grow in size while the AA (commensurate) stacked areas shrink. This relaxation is modelled in this report using techniques taken from continuum mechanics. Our model doesn't treat tBG in a fully atomistic way. Instead, we look at the continuous behaviour of tBG and see how the interlayer bonds and intralayer forces distort the continuum sheet where the physical atoms lie. A lot of the work done in modelling the electronic properties of tBG early on did not take into consideration this change in moiré pattern and assumed a rigid rotation. This lead to some discrepancy between different theoretical predictions of the *magic angle* and more recent experimental results (Jarillo-Herrero, P. et al. 2018). The theoretical prediction made by Bistritzer and MacDonald (2011) said that the first *magic angle* would lie at 1.05°. However, Tarnopolsky et al. (2019) corrected this assumption by taking into account the lattice relaxation effect and showed that the first *magic angle* is closer to 1.09° . This result agrees with the experimental result of 1.10° much more closely.

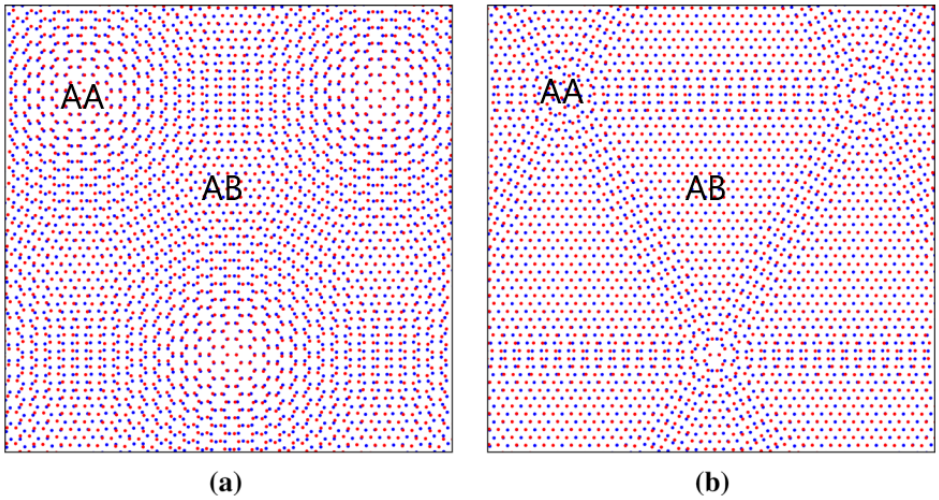

Figure 2: **a)** Rigidly rotated BG before relaxation. **b)** After relaxation, the moiré superlattice changes in such a way that the AA regions shrink while the AB regions expand (Paul Cazeaux, Mitchell Luskin & Daniel Massatt 2020).

To begin the formulation of our model, we first determine how a stacked 1D chain changes due to the interchain potential and in-plane elastic potentials. This model is numerically solved using Python 3.8, where the relative atomic displacement is calculated. Next, we formulate the theoretical basis necessary to generalise the model to a 2D system. Unfortunately, the calculations are challenging and inexact in their solution, meaning numerical methods have to be employed once again. More work is required to develop the model presented in this report fully. Particularly, numerical methods will have to be utilised to show the accuracy and usefulness of our model for 2D tBG.

The future of tBG and many similar materials is promising as they prove to be versatile in their application. Advances have been made in BG's friction and lubrication properties, where the low shear strength and weak interlayer interactions have shown that such 2D materials exhibit some incredibly low friction and wear-resisting properties on top of what is already mentioned (Liu et al. 2019). But above all, these materials give physicists a platform to explore quantum effects easily and cheaply.

2 Theory of superconductivity

Superconductivity has been a well-established phenomenon for over a century (Onnes 1911). Since then, scientists have searched for higher T_c (critical temperature at which the material becomes superconducting) superconductors (HTS) to help resolve our energy crisis and other related issues. At normal atmospheric pressure, the current highest T_c superconductor can operate at 139K (Dai et al. 1995). Until recently, this phenomenon has been associated with thermodynamic phase transitions, where temperature and pressure were the key variables in achieving superconduction.

The basic principle behind superconductivity is explained by Bardeen-Cooper-Schrieffer (BCS) theory (Bardeen, Cooper & Schrieffer 1957). In normal conductors, the charge carriers are electrons, which are half spin fermions. However, in superconductivity, the charge carriers are bosons called Cooper pairs. These are correlated states of two electrons that act like a particle. This delicate pairing can be easily interrupted by the thermal motion of electrons and nuclei. This explains why superconductivity is a low-temperature phenomenon. Pauli's exclusion principle says that two indistinguishable fermions cannot occupy the same quantum state in the same quantum system. But if the fermions pair up to produce a bosonic quasi-particle such as a Cooper pair (Cooper 1956), they can occupy the same quantum state. So in a superconductor, the Cooper-pairs exist at the lowest energy possible. This means that the system cannot lose any more energy as it is already at its lowest energy.

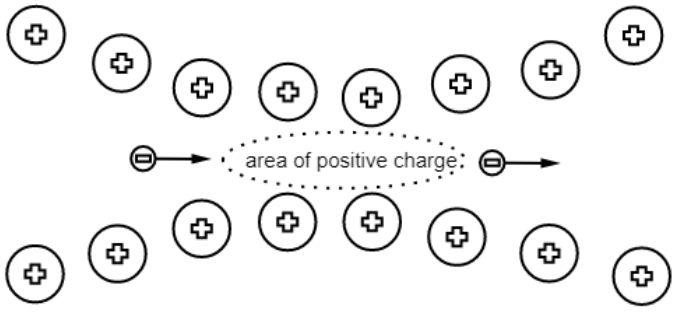

Figure 3: Diagram of a Cooper pair. This electron correlation can be broken by the thermal vibration of the charges, which explains the low temperature requirement for super conductivity.

Twisted bilayer graphene has shown that at low temperatures and specific twist angles it can also achieve superconductivity. This extra degree of freedom affords scientists a new avenue to explore this phenomenon and might give insights into new physics. There is some debate around whether or not tBG is a superconductor in the classical sense that BCS theory explains or if the underlying mechanism is completely novel. Recent experiments report the similarities between tBG and certain cuprates. Cuprates being the currently highest T_c superconductors, many hope that tBG will offer insight into HTS as it is precisely tunable in its rotation angle.

3 Method

3.1 Continuum mechanics and energy minimisation in 1D

To begin developing our model, we first consider a simple case of two stacked 1D chains of carbon atoms. The top chain has $N-1$ atoms, while the bottom has N atoms. We set periodic boundary conditions for the ends of our chains as we assume the chains are very long. The schematics of our set-up is shown in Figure 4. In the initial configuration, the atoms are spaced evenly. The goal is to determine how each layer affects one another and how the atoms will shift in response. The initial positions of each atom can be considered as our reference point. Two vectors then denote any shifting of the atoms with respect to their reference positions, $\boldsymbol{u}_1$ for the top layer and $\boldsymbol{u}_2$ for the bottom layer. But since we are only interested in their relative movements, we define a new function $\boldsymbol{\delta}$, which is equal to $\boldsymbol{\delta}(x) = ax/L_M + \boldsymbol{u}_2 - \boldsymbol{u}_1$. The first term takes into account the initial shift before relaxation takes place. The term L_M is the moiré length which is the distance between two AA stacked regions where the atoms lie perfectly on top of one another. For the 1D case, we assume the relative difference between the atoms is small, i.e. $a \approx a'$ and $L_m \gg a$. The $\boldsymbol{\delta}(x)$ function will then show us the interplay between the two layers.

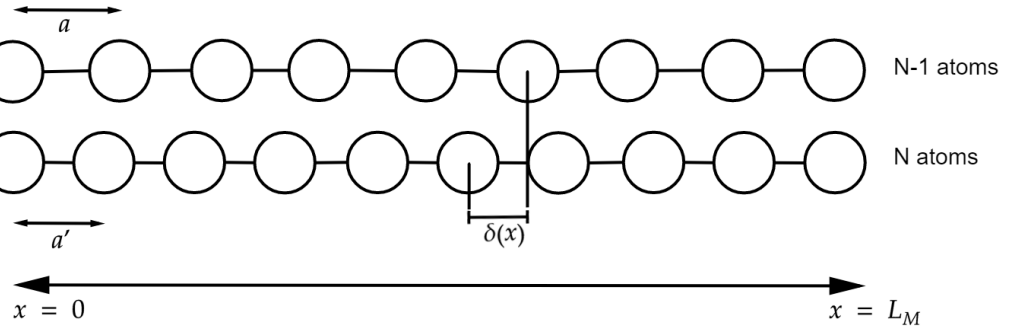

Figure 4: The schematics of our 1D continuum model for stacked chain of atoms.

We model the interlayer potential by the following cosine function:

$$V = -V_0 \cos\left(\frac{2\pi}{a}\boldsymbol{\delta}\right) \tag{1}$$

This means that when $\boldsymbol{\delta} = na$, $n \in \mathbb{N}$ the potential is minimised and when $\boldsymbol{\delta} = (n+1/2)a$ it is maximised with amplitude of V_0. The plot of this function is shown below in Figure 5.

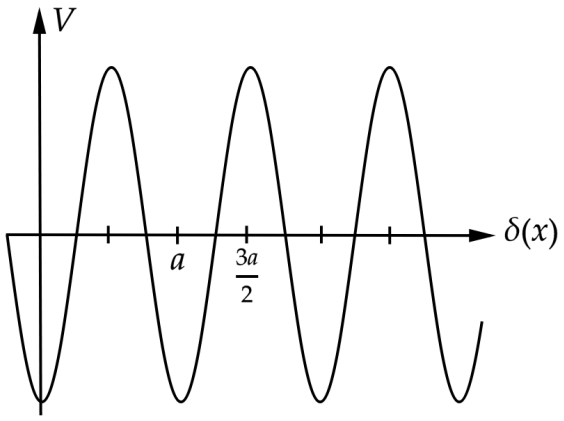

Figure 5: Plot of the potential V as a function of $\boldsymbol{\delta}$.

The total elastic potential is given by the following equation, where k denotes the spring constant:

$$
\begin{aligned}
U_{elastic} &= \int_{-\infty}^{\infty} \frac{k}{2} \left(\left(\frac{\partial \boldsymbol{u}_1}{\partial x} \right)^2 + \left(\frac{\partial \boldsymbol{u}_2}{\partial x} \right)^2 \right) dx \\
U_{binding} &= \int V(\boldsymbol{\delta})\, dx
\end{aligned}
\tag{2}
$$

Going back to equation (1), the interlayer binding energy is given by the following equation:
Now, we can write the total energy as the sum of the binding energy and the elastic potential energy as follows:

$$
U_{total} = \int_0^{L_M} \frac{k}{2} \left(\left(\frac{\partial \boldsymbol{u}_1}{\partial x} \right)^2 + \left(\frac{\partial \boldsymbol{u}_2}{\partial x} \right)^2 \right) dx - \int_0^{L_M} V_0 \cos\left(\frac{2\pi}{a} \left[\frac{ax}{L_M} + \boldsymbol{u}_2 - \boldsymbol{u}_1 \right] \right) dx \tag{3}
$$

We now want to see what values $\boldsymbol{u}_1$ and $\boldsymbol{u}_2$ will take in order to minimize the total energy. This means mathematically that we need to minimize the total energy using the Euler-Lagrange equation since we know that the system will take the configuration to have the least amount of energy possible. The Euler-Lagrange equation says that if we have $J = \int f(u, u', x)\, dx$ then J has stationary point if the following equation is satisfied:

$$
\frac{\partial f}{\partial u} - \frac{d}{dx} \left(\frac{\partial f}{\partial u'} \right) = 0 \tag{4}
$$

We will now define the following two vectors $\boldsymbol{u}_+$ and $\boldsymbol{u}_-$ as:

$$
\begin{aligned}
\boldsymbol{u}_+ &= \boldsymbol{u}_1 + \boldsymbol{u}_2 \\
\boldsymbol{u}_- &= \boldsymbol{u}_1 - \boldsymbol{u}_2
\end{aligned}
\tag{5}
$$

The reason for doing this is that now we can keep one of these two vectors to be constant, which will simplify our analysis. Going back to our total energy function, let W be the integrand of our total energy function.

$$
W = \frac{k}{2} \left(\left(\frac{\partial \boldsymbol{u}_1}{\partial x} \right)^2 + \left(\frac{\partial \boldsymbol{u}_2}{\partial x} \right)^2 \right) - V_0 \cos\left(\frac{2\pi}{a} \left[\frac{ax}{L_M} + \boldsymbol{u}_2 - \boldsymbol{u}_1 \right] \right) \tag{6}
$$

We can then apply the vectors from equation (6) to get the following:

$$W = \frac{k}{4}\left(\dot{\boldsymbol{u}}_+^2 + \dot{\boldsymbol{u}}_-^2\right) - V_0 \cos\left(G_m x - \frac{2\pi \boldsymbol{u}_-}{a}\right) \tag{7}$$

Note that we have $2\pi/L_M = G_m$, which is the reciprocal lattice vector length for the moiré superlattice and that the dot notation means a differentiation with respect to x.

Applying the Euler-Lagrange equation to W gives us:

$$\begin{aligned} \frac{\partial W}{\partial \boldsymbol{u}_+} - \frac{d}{dx}\left(\frac{\partial W}{\partial \dot{\boldsymbol{u}}_+}\right) = 0 \\ \frac{\partial W}{\partial \boldsymbol{u}_-} - \frac{d}{dx}\left(\frac{\partial W}{\partial \dot{\boldsymbol{u}}_-}\right) = 0 \end{aligned} \tag{8}$$

As mentioned earlier, to simplify the analysis, we set $\boldsymbol{u}_+$ to be constant. This is a trivial solution to the Euler-Lagrange equation and so we focus our attention to the second expression.
The last part of equation (9) once expanded out gives us the following equation:

$$\frac{2\pi}{a} V_0 \sin\left(G_m x - \frac{2\pi}{a}\boldsymbol{u}_-\right) + \frac{k}{2}\ddot{\boldsymbol{u}}_- = 0 \tag{9}$$

This is the final equation that we need to solve in order to figure out how the atoms have shifted with respect to one another.

3.1.1 Solving the 1D equation

Equation (10) is a non-linear second-order ODE, and thus we will use Discrete-Fourier-Transform (DFT) to solve it (see Appendix B). Firstly, we set our vector as a complex sum of Fourier coefficients as follows:

$$\boldsymbol{u}_-(x) = \sum_n u_n e^{inG_m x} \tag{10}$$

Next, we set the sin term to also be a sum with different Fourier coefficients.

$$\sin\left(G_m x - \frac{2\pi}{a}\boldsymbol{u}_-\right) = \sum_n f_n e^{inG_m x} \tag{11}$$

Putting equations (11) and (12) into equation (10) allows us to separate the first Fourier coefficients in terms of the second Fourier coefficients, giving us the following:

$$u_n = -\frac{4\pi V_0}{akn^2 G_m^2} f_n \tag{12}$$

This problem is then solved numerically in Python 3.8. We will initially have a guess solution for the f_n coefficients in equation (12). We get this by performing inverse DFT on some test function. Next, we put the coefficients into equation (13) to determine u_n, and plug those into equation (11). Lastly, we put the $\boldsymbol{u}_-$ that we get back into equation (12). The equality will not hold but that is fine as we expect an approximate solution. So, we set a certain tolerance level for our guess solution, so that we can keep the f_n coefficients that are within the tolerance level as our final solution. It is worth noting that we don't have to start with f_n in order to solve this problem. We could have started with u_n and do a similar loop. The main point is that the problem is solved self-consistently and that the solution will be approximate which involves some initial guess work. Once we have $\boldsymbol{u}_-$, we can get back the function $\boldsymbol{\delta}(x)$. Plotting this function will tell us how the atoms move relative to each other.

3.2 Generalisation to 2D

The hexagonal lattice of graphene is shown in Figure 6a and its reciprocal lattice is shown in Figure 6b. The two vectors in Figure 6a denote the Bravais lattice vectors. We choose our coordinate system so that $\boldsymbol{a}_1 = a(1,0)$ and $\boldsymbol{a}_2 = \frac{a}{2}(1,\sqrt{3})$. For graphene it is known that $a = 0.246$ nm.

We can find the reciprocal lattice vectors easily from looking at the diagram in Figure 6b. The vector $\boldsymbol{a}_1^* \propto (\cos(30°), -\sin(30°))$. So we get:

$$\begin{aligned} \boldsymbol{a}_1^* &= \frac{2\pi}{a}\left(1, -\frac{1}{\sqrt{3}}\right) \\ \boldsymbol{a}_2^* &= \frac{2\pi}{a}\left(0, \frac{2}{\sqrt{3}}\right) \end{aligned} \tag{13}$$

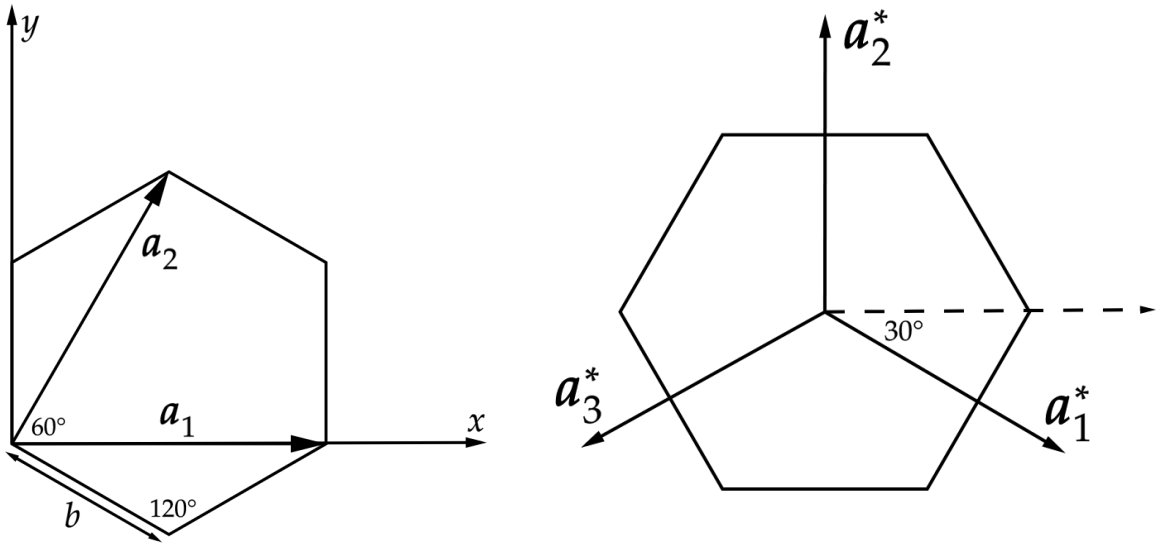

(a) (b)

Figure 6: **(a)** The real lattice (Bravais) of graphene where the two vectors denote the lattice vectors. **(b)** The reciprocal lattice of graphene. The vectors with * are the reciprocal lattice vectors.

We set the third vector as $\boldsymbol{a}_3^* = -\boldsymbol{a}_1^* - \boldsymbol{a}_2^*$, which means:

$$\boldsymbol{a}_3^* = \frac{2\pi}{a}\left(-1, -\frac{1}{\sqrt{3}}\right) \tag{14}$$

From here, we look at the displacement of each atom in the real lattices for both types of stacking. A small displacement in AA stacked BG is shown in Figure 7a and AB/BA stacked BG is shown in Figure 7b.

We want the interlayer potential to be maximum when the atoms are stacked in AA configuration and we want the potential to be minimum when the atoms are stacked in AB configuration. The vectors $\boldsymbol{u}^{(i)}(\vec{r})$ keep track of the displacements of each point where the superscript i tells us the layer the vector corresponds to. The term δ_{AB} is the displacement for a full AB stacked BG and it is calculated in terms of the lattice vectors, i.e. $\boldsymbol{a}_1$ and $\boldsymbol{a}_2$ are our basis vectors. We can see that $\delta_{AB} = (a/2, a/(2\sqrt{3}))$. We then define the interlayer potential that fulfills our requirements that we set out above. We let the potential to be:

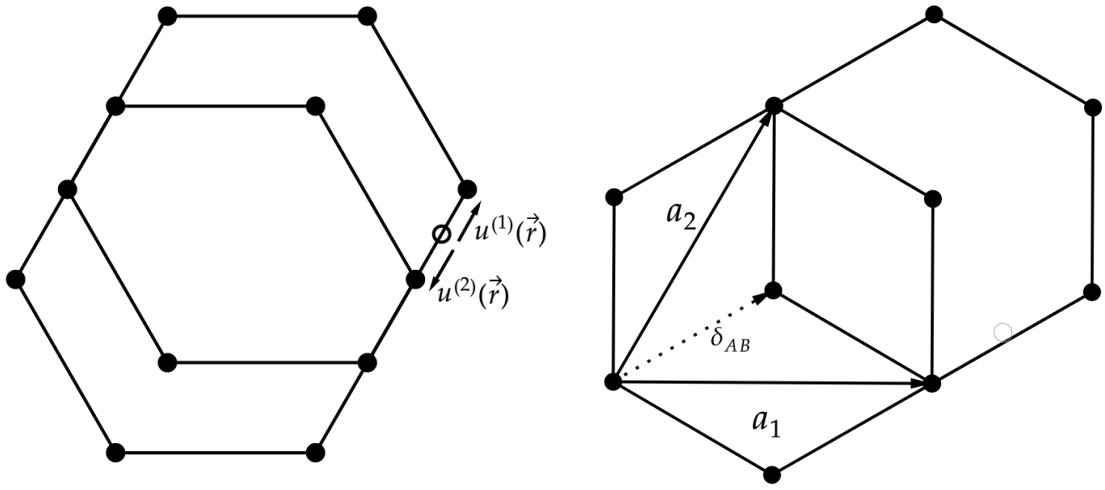

(a) (b)

Figure 7: **(a)** Small perturbation of carbon atoms from their reference position in AA stacked BG. **(b)** Displacement of the atoms when the stacking becomes AB.

$$V(\boldsymbol{\delta}) = 2V_0 \sum_i \cos(\boldsymbol{a}_i^* \cdot \boldsymbol{\delta}) \tag{15}$$

This fulfills our conditions as $V(0) = 6V_0$, which is a maximum that corresponds to AA stacked BG and $V(\delta_{AB}) = -3V_0$ which is a minimum and it corresponds to AB stacked BG.

The elastic potential is given by the following equation (for the derivation see Appendix A):

$$\Delta F = \frac{K_A}{2}(u_{xx} + u_{yy})^2 + \mu \left(\frac{(u_{xx} - u_{yy})^2}{2} + 2u_{xy}^2 \right) \tag{16}$$

We add our potential function equation (16) on top of the elastic energy to get the total energy. But first we can define two more vectors as we did in the 1D case to keep track of the relative displacements between the layers. This way we don't have to track the displacements for both layers from some initial reference points. We let:

$$\begin{aligned} \boldsymbol{u}^{(1)} + \boldsymbol{u}^{(2)} &= \boldsymbol{u}_+ \\ \boldsymbol{u}^{(1)} - \boldsymbol{u}^{(2)} &= \boldsymbol{u}_- \end{aligned} \tag{17}$$

We can also define the $\boldsymbol{\delta}$ function as $\boldsymbol{\delta}(\vec{r}) = \delta_{AB} + \boldsymbol{u}^{(2)} - \boldsymbol{u}^{(1)} \equiv \delta_{AB} - \boldsymbol{u}_-$. Before we add up the terms to get the total energy, we first need to know how the terms in equation (17) relate to the two vectors we just defined. These terms relate as follows:

$$\begin{aligned} u_{xx} &= \frac{\partial u_x}{\partial x} \\ u_{yy} &= \frac{\partial u_y}{\partial y} \\ u_{xy} &= \frac{1}{2}\left(\frac{\partial u_x}{\partial y} + \frac{\partial u_y}{\partial x}\right) \end{aligned} \tag{18}$$

So, we can now write the total energy equation, which is simply the sum of equation (16) and equation (17):

$$U_{total} = \frac{K_A}{2}(u_{xx} + u_{yy})^2 + \mu\left(\frac{(u_{xx} - u_{yy})^2}{2} + 2u_{xy}^2\right) + 2V_0 \sum_i \cos(\boldsymbol{a}_i^* \cdot \boldsymbol{\delta}) \tag{19}$$

We then replace the u_{ij} terms in the elastic potential part with the terms from equation (19). We can also perform the summation in the interlayer potential term which gives us the following:

$$\begin{aligned} U_{total} = {} & \frac{K_A}{2}\left(\frac{\partial u_x}{\partial x} + \frac{\partial u_y}{\partial y}\right)^2 + \mu\left[\frac{1}{2}\left(\frac{\partial u_x}{\partial x} - \frac{\partial u_y}{\partial y}\right)^2 + \frac{1}{2}\left(\frac{\partial u_x}{\partial y} + \frac{\partial u_y}{\partial x}\right)^2\right] \\ & + 2V_0\left\{\cos\left(\frac{2\pi}{3} - \frac{2\pi}{a}\left[u_-^x - \frac{u_-^y}{\sqrt{3}}\right]\right) + \cos\left(\frac{2\pi}{3} - \frac{4\pi}{a\sqrt{3}u_-^y}\right) + \cos\left(\frac{2\pi}{a}\left[u_-^x + \frac{u_-^y}{\sqrt{3}}\right] - \frac{4\pi}{a}\right)\right\} \end{aligned} \tag{20}$$

Note that $u_- = (u_-^x, u_-^y)$, $u_x = u_1^x + u_2^x$, and $u_y = u_1^y + u_2^y$. Using this, we can now rewrite the total energy in terms of $\boldsymbol{u}_+ = (u_+^x, u_+^y)$ and $\boldsymbol{u}_- = (u_-^x, u_-^y)$.

After some lengthy algebra, we get the elastic term to be equal to the following (see Appendix C):

$$\begin{aligned} U_{elastic} = \frac{K_A}{4}\left[\left(\frac{\partial u_+^x}{\partial x}+\frac{\partial u_+^y}{\partial y}\right)^2+\left(\frac{\partial u_-^x}{\partial x}+\frac{\partial u_-^y}{\partial y}\right)^2\right]+\frac{\mu}{4}\left\{\left(\frac{\partial u_+^x}{\partial x}\right)^2+\left(\frac{\partial u_-^x}{\partial x}\right)^2\right. \\ \left.+\left(\frac{\partial u_+^y}{\partial y}\right)^2+\left(\frac{\partial u_-^y}{\partial y}\right)^2+\left(\frac{\partial u_+^x}{\partial y}\right)^2+\left(\frac{\partial u_-^x}{\partial y}\right)^2+\left(\frac{\partial u_+^y}{\partial x}\right)^2+\left(\frac{\partial u_-^y}{\partial x}\right)^2\right\} \end{aligned} \tag{21}$$

The potential term is already in terms of $\boldsymbol{u}_+$ and $\boldsymbol{u}_-$, so we can add it to equation (22) to get the total energy U_{total}. Notice that the total energy, which we will simply call U for simplicity is a function of u_+^x, u_+^y, u_-^x, and u_-^y. To minimize the total energy, we need to solve the following Euler-Lagrange equations:

$$\frac{\partial U}{\partial u_-^x}-\frac{d}{dx}\left(\frac{\partial U}{\partial u_-^{xx}}\right)-\frac{d}{dy}\left(\frac{\partial U}{\partial u_-^{xy}}\right)=0 \tag{22}$$

$$\frac{\partial U}{\partial u_-^y}-\frac{d}{dx}\left(\frac{\partial U}{\partial u_-^{yx}}\right)-\frac{d}{dy}\left(\frac{\partial U}{\partial u_-^{yy}}\right)=0 \tag{23}$$

where $u_-^{xx}=\frac{\partial u_-^x}{\partial x}$ and $u_-^{yx}=\frac{\partial u_-^y}{\partial x}$ and so forth.

Once again after some lengthy algebra, equation (23) becomes the following:

$$\begin{aligned} 0 = \frac{4\pi}{a}V_0\left[\sin\left(\frac{2\pi}{3}-\frac{2\pi}{a}\left\{u^x-\frac{u^y}{\sqrt{3}}\right\}\right)-\sin\left(-\frac{4\pi}{3}+\frac{2\pi}{a}\left\{u^x+\frac{u^y}{\sqrt{3}}\right\}\right)\right] \\ -\frac{K_A}{2}\left(\frac{\partial^2 u^x}{\partial x^2}+\frac{\partial^2 u^y}{\partial x\partial y}\right)-\frac{\mu}{2}\left(\frac{\partial^2 u^x}{\partial x^2}+\frac{\partial^2 u^x}{\partial y^2}\right) \end{aligned} \tag{24}$$

Note that we have dropped the '-' from the subscript as it is no longer necessary since we don't have any of the '+' terms left. As in the 1D case, we set $\boldsymbol{u}^+$ to be constant to simplify the analysis. This means that there are two additional equations, similar to equation (22) and equation (23) but in terms of $\boldsymbol{u}^+$ which we will ignore. Performing the same calculations on equation (24) gives us the following:

$$0 = -\frac{4\pi}{a\sqrt{3}}V_0\left[\sin\left(\frac{2\pi}{3} - \frac{2\pi}{a}\left\{u^x - \frac{u^y}{\sqrt{3}}\right\}\right) - 2\sin\left(\frac{2\pi}{3} - \frac{4\pi}{a\sqrt{3}}u^y\right)\right.$$
$$\left. + \sin\left(-\frac{4\pi}{3} + \frac{2\pi}{a}\left\{u^x + \frac{u^y}{\sqrt{3}}\right\}\right)\right] - \frac{\mu}{2}\left(\frac{\partial^2 u^y}{\partial x^2} + \frac{\partial^2 u^y}{\partial y^2}\right) - \frac{K_A}{2}\left(\frac{\partial^2 u^x}{\partial y \partial x} + \frac{\partial^2 u^y}{\partial y^2}\right) \tag{25}$$

We now need to solve equation (25) and equation (26) in order to see how the atoms in our BG move with respect to each other.

3.2.1 Solving the 2D equation

The general strategy of solving equation (25) and equation (26) is the same as in the 1D case. We want to make a self-consistent loop that requires an initial guess. Unlike the 1D case, we now need to take into consideration the rotation angle between the two layers. First, we write our $\boldsymbol{u}$ vector as a Fourier sum as follows:

$$\boldsymbol{u}(x,y) = \sum_{\boldsymbol{q}} \boldsymbol{u}_{\boldsymbol{q}} e^{i\boldsymbol{q}\cdot\boldsymbol{r}} = \sum_{\boldsymbol{q}} \boldsymbol{u}_{q_x} e^{i(q_x x + q_y y)} + \sum_{\boldsymbol{q}} \boldsymbol{u}_{q_y} e^{i(q_x x + q_y y)} \tag{26}$$

Here, $\boldsymbol{q} = (q_x, q_y) = m_1\boldsymbol{G}_1^M + m_2\boldsymbol{G}_2^M$, where $m_i \in \mathbb{Z}$. Thus, the summation over $\boldsymbol{q}$ means adding up all allowed combinations of integers m_1 and m_2. These integers denote the lattice points in the reciprocal moiré lattice which is shown in Figure 8 below.

The basis vectors $\boldsymbol{G_i^M}$ are given by $\boldsymbol{G_1^M} = G_M(1,0)$ and $\boldsymbol{G_2^M} = G_M(-1/2, \sqrt{3}/2)$, where $G_m = 2\pi/L_M$ with L_M being the moiré length.

Next, we rewrite the sin terms in our interlayer potential as a Fourier sum as follows:

$$\sin(\boldsymbol{G}_j^M \cdot \boldsymbol{r} + \boldsymbol{a}_j^* \cdot \boldsymbol{u}) = \sum_{\boldsymbol{q}} f_{\boldsymbol{q}}^j e^{i\boldsymbol{q}\cdot\boldsymbol{r}} \tag{27}$$

Here, j takes the values 1, 2 and 3 and the term $\boldsymbol{G_3^M} = -\boldsymbol{G_1^M} - \boldsymbol{G_2^M}$. The rotation angle comes into play in our model when we calculate the moiré lattice length. It is known that $L_M = \frac{a}{2\sin(\theta/2)}$ (Shallcross, Kandelaki & Pankratov 2010), where a is the distance between neighbouring carbon atoms in normal

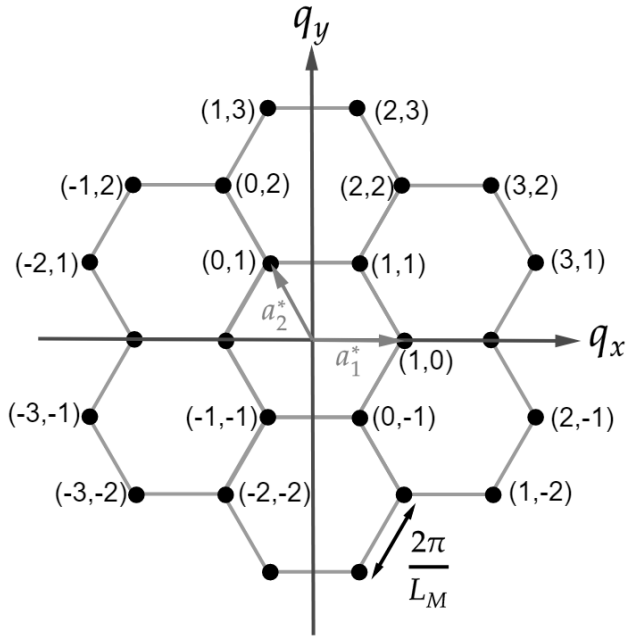

Figure 8: Reciprocal moiré lattice points, denoted by integer pairs.

graphene and θ is the relative twist angle between the two graphene layers. As discussed earlier, θ is small for the first *magic angle*, only around 1.10°.

The next step in our calculations is rewriting equation (24) and equation (25) in terms of our Fourier coefficients from equation (26). After some lengthy algebra with partial derivatives (see Appendix D), we arrive at the following two equations:

$$\frac{4\pi V_0}{a}\left[\sum_{\boldsymbol{q}} f_{\boldsymbol{q}}^3 - \sum_{\boldsymbol{q}} f_{\boldsymbol{q}}^1\right] = \sum_{\boldsymbol{q}} \boldsymbol{u}_{q_x}\left(\frac{K_A}{2}q_x^2 + \frac{\mu}{2}q_x^2 - \frac{\mu}{2}q_y^2\right) + \frac{K_A}{2}\sum_{\boldsymbol{q}} \boldsymbol{u}_{q_y} q_x q_y \tag{28}$$

$$\frac{4\pi V_0}{a\sqrt{3}}\left[\sum_{\boldsymbol{q}} f_{\boldsymbol{q}}^1 - 2\sum_{\boldsymbol{q}} f_{\boldsymbol{q}}^2 + \sum_{\boldsymbol{q}} f_{\boldsymbol{q}}^3\right] = \sum_{\boldsymbol{q}} \boldsymbol{u}_{q_x}\left(\frac{K_A}{2}q_x q_y\right) - \sum_{\boldsymbol{q}} \boldsymbol{u}_{q_y}\left(\frac{\mu}{2}q_y^2 - \frac{K_A}{2}q_y^2 - \frac{\mu}{2}q_x^2\right) \tag{29}$$

We can rewrite our result as a matrix multiplication after making a small substitution, where we let $K_A = \lambda + \mu$ as the parameters λ and μ are known for graphene. These two parameters are known

as *Lamé's first parameter* and *Lamé's second parameter* respectively. These are material dependent parameters with the same units as stress and is often given in terms of [Pa]. The combined matrix form is as follows:

$$\begin{bmatrix} \left(\frac{\lambda}{2}+\frac{2\mu}{2}\right)q_x^2-\frac{\mu}{2}q_y^2 & \frac{\lambda+\mu}{2} \\ \frac{\lambda+\mu}{2} & \left(\frac{\lambda}{2}+\frac{2\mu}{2}\right)q_y^2-\frac{\mu}{2}q_x^2 \end{bmatrix} \cdot \begin{bmatrix} \boldsymbol{u}_{q_x} \\ \boldsymbol{u}_{q_y} \end{bmatrix} = \begin{bmatrix} \frac{4\pi V_0}{a}\left[\sum_{\boldsymbol{q}} f_{\boldsymbol{q}}^3 - \sum_{\boldsymbol{q}} f_{\boldsymbol{q}}^1\right] \\ \frac{4\pi V_0}{a\sqrt{3}}\left[\sum_{\boldsymbol{q}} f_{\boldsymbol{q}}^1 - 2\sum_{\boldsymbol{q}} f_{\boldsymbol{q}}^2 + \sum_{\boldsymbol{q}} f_{\boldsymbol{q}}^3\right] \end{bmatrix} \tag{30}$$

We will call this symmetric matrix $M_{\boldsymbol{q}}$, and so this multiplication has the form:

$$M_{\boldsymbol{q}} \cdot \boldsymbol{u}_q = \sum_j 4V_0 f_{\boldsymbol{q}}^j \boldsymbol{a}_j^* \tag{31}$$

To get the self-consistent solution, we will look at equation (26), equation (27) and equation (31). We can first guess the term $\boldsymbol{u}$ inside the sin in equation (27). Then, we can do inverse DFT to get the complex Fourier coefficients $f_{\boldsymbol{q}}^j$. Next, we can construct the left side of equation (31) and multiply it by the inverse of our matrix, $M_{\boldsymbol{q}}^{-1}$. From here, we get back the Fourier coefficients $\boldsymbol{u}_{\boldsymbol{q}}$. Using equation (26), we can then get back our vector $\boldsymbol{u}$. Finally, we compare these values with our initial guess values and only keep the guess values of $\boldsymbol{u}$ that are within some tolerance level to the final values of $\boldsymbol{u}$. Remember that $\boldsymbol{u}$ is equal to $\boldsymbol{u}_-$. Once we have this, we can get back the displacement vectors from equation (17) and we will be able to simulate the displacements of our carbon atoms in our tBG when they are relaxed.

4 Results

4.1 Numerical solutions for the 1D model

The equations from 1D continuum model (section 3.1.1) were solved in Python 3.8 as outlined in that section. This means we solved the problem self-consistently, using equation (10), equation (11) and equation (12). The parameters that we varied were V_0, the strength of the interlayer potential and k, the in-plane elastic potential strength. The parameters that were kept constant throughout the simulations are L_M, length of our 1D chains, and a, the inter-atomic distance for the top chain. The first result is shown in Figure 9a. For our guess solution, we sampled a simple sin function to generate the guesses.

We weren't that stringent in our tolerance as it was kept at a rather high value of 0.1. Here, the in-plane elastic potential is quite weak, and so the atoms in the top chain are spaced out quite evenly. The plot of $\delta(x)$ and the potential function is shown. The schematics of what the chain would look like is then shown in Figure 9b.

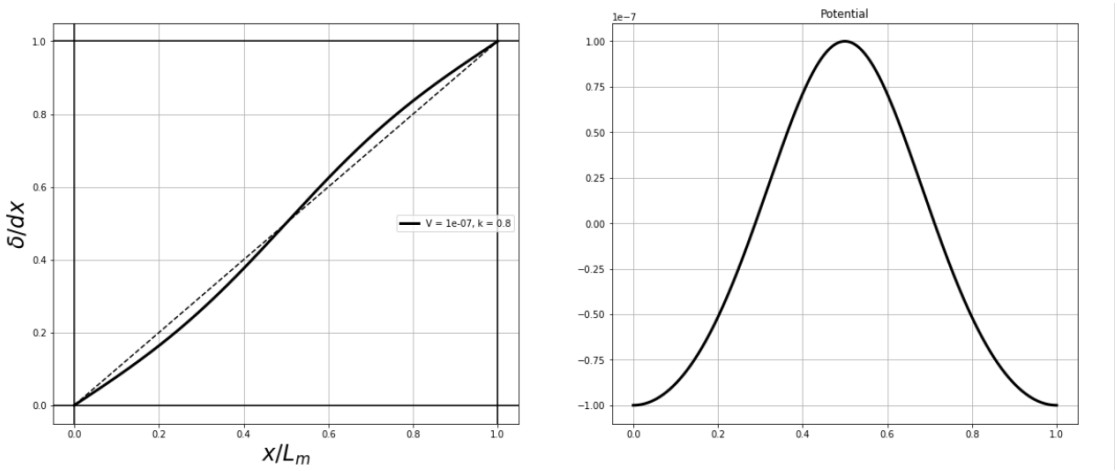

(a)

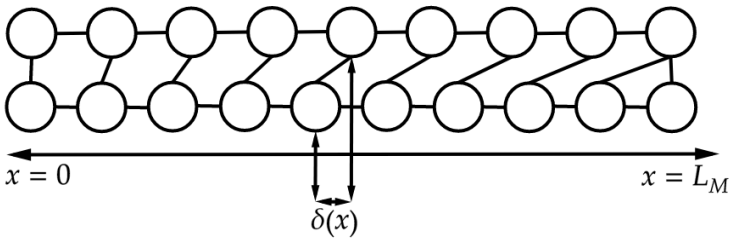

(b)

Figure 9: **(a)** The results from the simulations where the in-plane coupling is strong compared to the interlayer potential. **(b)** Diagram of what the chains would look like in this situation.

In the next simulation, we made the in-plane elastic coupling 4 times weaker, while we increased the interlayer potential strength by a factor of 5. The results are shown in Figure 10.

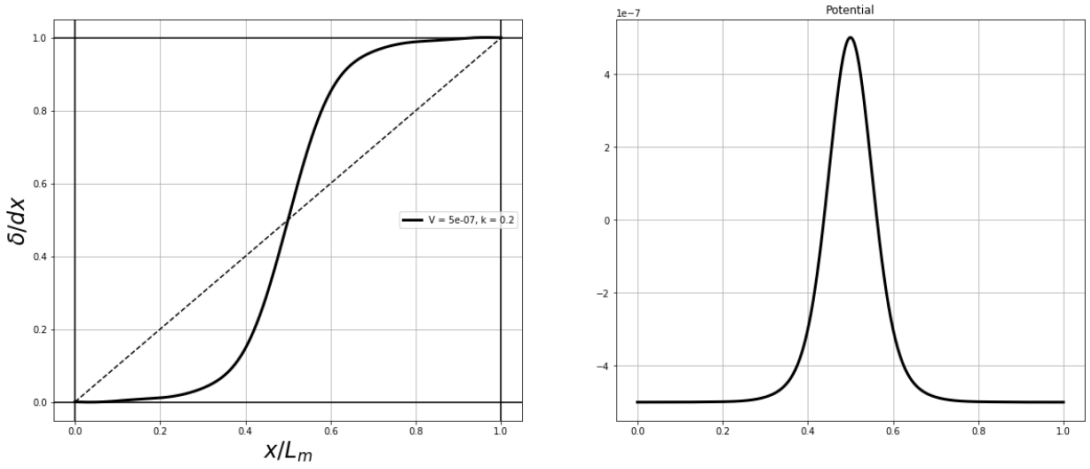

(a)

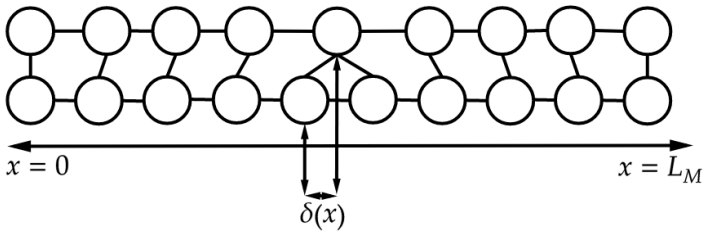

(b)

Figure 10: **(a)** The in-plane elastic potential has been reduced substantially by a factor of 4, while the interlayer potential strength was increased by a factor of 5. **(b)** Diagram of what the chains would look like in this scenario. Notice how the atoms on the top chain are packed tightly on each ends. The displacement is only big in the middle, where the interlayer potential is much more concentrated.

In the last simulation, we increase the interlayer potential even further, by a factor of 9, compared to the scenario in Figure 9. We also reduce the in-plane elastic potential by a factor of 8 compared to the same scenario. The results are plotted in Figure 11a, and the diagram for the chains is shown in Figure 11b below.

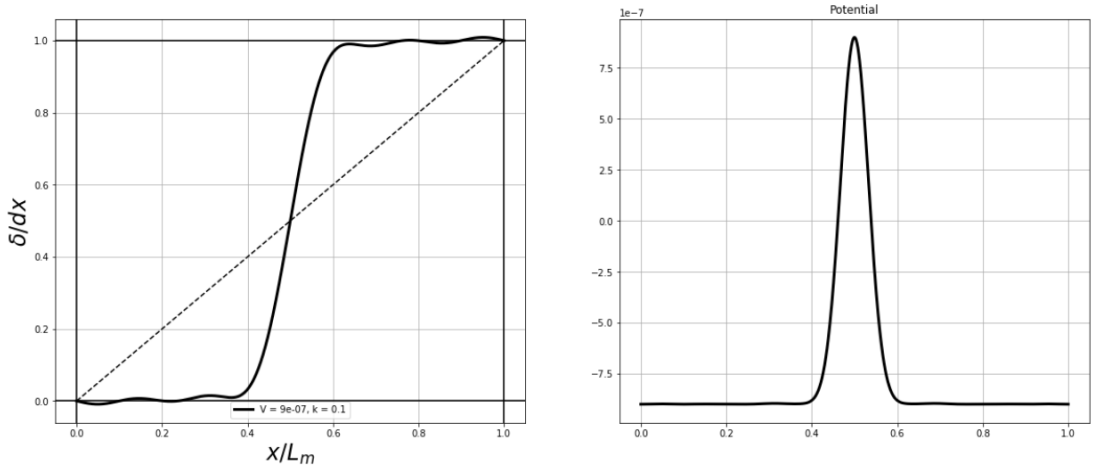

(a)

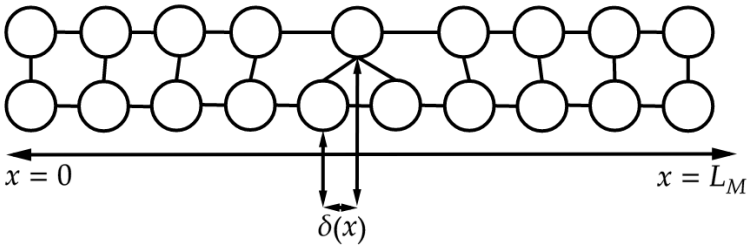

(b)

Figure 11: **(a)** The in-plane elastic potential has been reduced substantially by a factor of 8 compared to Figure 9, while the interlayer potential strength was increased by a factor of 9. **(b)** Diagram of what the chains would look like in this scenario. Notice how the atoms on the top chain are packed even more tightly on each ends. The displacement is only big in the middle as before, where the interlayer potential is much more narrow.

It is clear that if we keep making the interlayer potential stronger, the plot will more and more closely approximate a sort of step function. But, we know that the interlayer coupling is weak in graphene, and so it is useful to keep the in-plane potential relatively large. For a large in-plane potential, the plot will simply approximate a straight line and the chains would look close to what we have in Figure 4. It isn't clear why we see a small oscillatory behaviour in Figure 11a. It could be due to some noise introduced in the simulation process and thus requires further investigation.

4.2 Expected solutions for the 2D model

We expect the general solution to our 2D model to show AA stacked regions in the tBG shrinking and AB regions growing in size. The degree to which this happens will depend on the parameter values that we set. Fully atomistic calculations done by Wijk et al. (2015) show that the hexagonal patterns change to produce triangular lattices in the moire superlattice. This is due to the AA and AB areas changing in size. The simulation is shown in Figure 12 below. The vector field in Figure 12c shows the displacement of atoms as a result of the tBG relaxing.

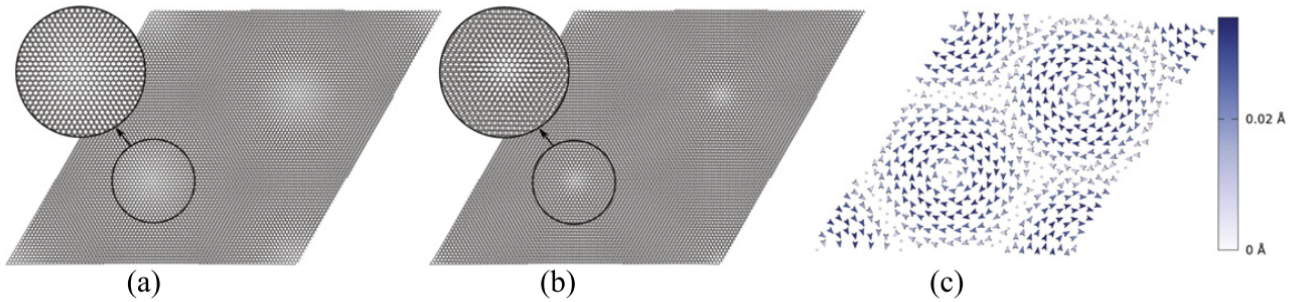

Figure 12: The rotation angle was reported to be $\theta = 1.2°$ and $a = 115.3\mathring{A}$. **(a)** The tBG before relaxation (rigid rotation). **(b)** The tBG after relaxation. **(c)** The arrows indicate direction, while the color indicates the size of the atomic displacements. For visualization purposes the authors set $\theta = 5.7°$ and $a = 24.5\mathring{A}$.

5 Conclusion

We showed in this report how weak interlayer coupling of twisted bilayer graphene could nevertheless play an important role in distorting and displacing the atoms from their initial positions of the perfectly aligned hexagonal lattice. Furthermore, these small displacements vary the shape and size of the moiré pattern that the tBG produces. We modelled this "relaxation" effect using the continuum mechanics approach where the individual atoms were not considered. Instead, we treated the entire graphene sheet as an interacting entity and tried to model its reaction to the other layer. Our model was formulated from a simple 1D case and was generalised to a sophisticated 2D case. Some basic assumptions were baked into the model, such as how the relative twist angle is small, about $1.10°$. This angle is the first *magic angle* of tBG, where superconductivity is first achieved near absolute zero. While there are plenty of superconducting materials at such low temperatures, tBG gives physicists the option to turn the superconductivity on and off at will by controlling the twist angle. This additional degree of freedom is crucial as it paves the way toward a cheaper and easily accessible superconductor.

6 References

Bardeen, J., Cooper, L.N. and Schrieffer, J.R. (1957). Theory of Superconductivity. Physical Review, 108(5), pp.1175–1204.

Bistritzer, R. and MacDonald, A.H. (2011). Moiré bands in twisted double-layer graphene. Proceedings of the National Academy of Sciences, 108(30), pp.12233–12237.

Cao, Y., Fatemi, V., Fang, S., Watanabe, K., Taniguchi, T., Kaxiras, E. and Jarillo-Herrero, P. (2018). Unconventional superconductivity in magic-angle graphene superlattices. Nature, [online] 556(7699), pp.43–50. Available at: https://www.nature.com/articles/nature26160.

Cao, Y., Luo, J. Y., Fatemi, V., Fang, S., Sanchez-Yamagishi, J. D., Watanabe, K., Taniguchi, T., Kaxiras, E. and Jarillo-Herrero, P. (2016). Superlattice-Induced Insulating States and Valley-Protected Orbits in Twisted Bilayer Graphene. Physical Review Letters, 117(11).

Cazeaux, P., Luskin, M. and Massatt, D. (2019). Energy Minimization of Two Dimensional Incommensurate Heterostructures. Archive for Rational Mechanics and Analysis, 235(2), pp.1289–1325.

Cooper, L.N. (1956). Bound Electron Pairs in a Degenerate Fermi Gas. Physical Review, 104(4), pp.1189–1190.

Dai, P., Chakoumakos, B.C., Sun, G.F., Wong, K.W., Xin, Y. and Lu, D.F. (1995). Synthesis and neutron powder diffraction study of the superconductor HgBa2Ca2Cu3O8 + δ by Tl substitution. Physica C: Superconductivity, 243(3-4), pp.201–206.

Delhaes P. (2001). Graphite and precursors. Amsterdam: Gordon & Breach.

Green, T.A. Weigle, J (1948). Helv. Phys. Acta 21, 217

He, F., Zhou, Y., Ye, Z., Cho, S.-H., Jeong, J., Meng, X. and Wang, Y. (2021). Moiré Patterns in 2D Materials: A Review. ACS Nano, 15(4), pp.5944–5958.

Kim, K., Yankowitz, M., Fallahazad, B., Kang, S., Movva, H.C.P., Huang, S., Larentis, S., Corbet, C.M., Taniguchi, T., Watanabe, K., Banerjee, S.K., LeRoy, B.J. and Tutuc, E. (2016). van der Waals Heterostructures with High Accuracy Rotational Alignment. Nano Letters, 16(3), pp.1989–1995.

Liu, L., Zhou, M., Jin, L., Li, L., Mo, Y., Su, G., Li, X., Zhu, H. and Tian, Y. (2019). Recent advances in friction and lubrication of graphene and other 2D materials: Mechanisms and applications. Friction, 7(3), pp.199–216.

Lopes dos Santos, J.M.B., Peres, N.M.R. and Castro Neto, A.H. (2012). Continuum model of the twisted graphene bilayer. Physical Review B, 86(15).

Nguyen, V.-H., Paszko, D., Lamparski, M., Van Troeye, B., Meunier, V. and Charlier, J.-C. (2021). Electronic localization in small-angle twisted bilayer graphene. 2D Materials.

Novoselov, K.S. (2004). Electric Field Effect in Atomically Thin Carbon Films. Science, [online] 306(5696), pp.666–669. Available at: https://science.sciencemag.org/content/306/5696/666.full.

Onnes, H.K. (1911) The Superconductivity of Mercury. Comm. Phys. Lab. Univ., Leiden, 122-124

Shallcross, S., Sharma, S., Kandelaki, E. and Pankratov, O.A. (2010). Electronic structure of turbostratic graphene. Physical Review B, 81(16).

Tarnopolsky, G., Kruchkov, A.J. and Vishwanath, A. (2019). Origin of *magic angle*s in Twisted Bilayer Graphene. Physical Review Letters, 122(10).

Wijk, M.M. van, Schuring, A., Katsnelson, M.I. and Fasolino, A. (2015). Relaxation of moiré patterns for slightly misaligned identical lattices: graphene on graphite. 2D Materials, 2(3), p.034010.

7 Appendix

A. Elasticity in 2D

u_{ij} - strain tensor

$$u_{ij} = \frac{1}{2}\left(\frac{\partial u_i}{\partial x_j} + \frac{\partial u_j}{\partial x_i} + \left(\sum_k \frac{\partial u_k}{\partial x_i}\frac{\partial u_k}{\partial x_j}\right)\right) \tag{32}$$

Small deformation $\implies$ drop the summation term.

$$u_{ij} = \frac{1}{2}\left(\frac{\partial u_i}{\partial x_j} + \frac{\partial u_j}{\partial x_i}\right) \tag{33}$$

σ_{ij} - stress tensor (force per unit area)

$$F_i = \sum_j \sigma_{ij} a_j \tag{34}$$

General form of Hooke's law (C_{ijkl} - set of elastic constants)

$$\sigma_{ij} = \sum_{ij} C_{ijkl} u_{kl} \tag{35}$$

The formula for the free energy

$$\Delta F = \frac{1}{2}\sum_{ijkl} C_{ijkl} u_{ij} u_{kl} \tag{36}$$

Our setup has 6-fold symmetry. We introduce a new coordinate system: $\xi = x + iy$ and $\eta = x - iy$. A rotation about the origin in the xy plane by an angle θ changes ξ and η by:

$$\begin{aligned} \xi &\to \xi e^{i\theta} \\ \eta &\to \eta e^{-i\theta} \end{aligned} \tag{37}$$

We want an it to be invariant for $\theta = 30°$.

$$\Delta F = 2C_{\xi\eta\xi\eta}u_{\xi\eta}u_{\xi\eta} + C_{\xi\xi\eta\eta}u_{\xi\xi}u_{\eta\eta} \tag{38}$$

We make the substitution that $u_{\xi\xi} = u_{xx} - u_{yy} + 2iu_{xy}$, $u_{\eta\eta} = u_{xx} - u_{yy} - 2iu_{xy}$ and $u_{\xi\eta} = u_{xx} + u_{yy}$. This gives the energy to be:

$$\Delta F = \frac{K_A}{2}(u_{xx} + u_{yy})^2 + \mu\left(\frac{(u_{xx} - u_{yy})^2}{2} + 2u_{xy}^2\right) \tag{39}$$

Here, K_A is the are compression modulus and μ is the shear modulus.

(Note: This derivation is taken from Boal, D. H. (2002). Mechanics of the cell. Cambridge University Press.)

B. Discrete Fourier Transform

Fourier Transform

(time $\rightarrow$ frequency):

$$\mathcal{F}(j\omega) = \int_{-\infty}^{\infty} f(t) e^{-j\omega t} dt \tag{40}$$

(frequency $\rightarrow$ time)

$$f(t) = \frac{1}{2\pi} \int_{-\infty}^{\infty} \mathcal{F}(j\omega) e^{j\omega t} d\omega \tag{41}$$

Discrete Fourier Transform and inverse DFT

$$\begin{aligned} \mathcal{X} &= \sum_{n=0}^{N-1} x(n) e^{-j\frac{2\pi}{N}kn} \\ x(n) &= \frac{1}{N} \sum_{n=0}^{N-1} e^{j\frac{2\pi}{N}kn} \end{aligned} \tag{42}$$

Discrete Time Fourier Transform

$$\begin{aligned} \mathcal{X}(j\omega) &= \sum_{n=-\infty}^{\infty} x(n) e^{-jn\omega} \\ x(n) &= \frac{1}{2\pi} \int_{-\frac{T}{2}}^{\frac{T}{2}} \mathcal{X}(j\omega) e^{jn\omega} d\omega \end{aligned} \tag{43}$$

C. Deriving the elastic potential in 2D

This derivation shows how the elastic term in equation (20) becomes equal to equation (21). Note that the superscripts 1 and 2 here refer to the layers, not exponents.

Starting equation:

$$U_{elastic} = \frac{K_A}{2}\left[\left(\frac{\partial u_x^1}{\partial x}+\frac{\partial u_y^1}{\partial y}\right)^2+\left(\frac{\partial u_x^2}{\partial x}+\frac{\partial u_y^2}{\partial y}\right)^2\right]+\frac{\mu}{2}\left[\left(\frac{\partial u_x^1}{\partial x}-\frac{\partial u_y^1}{\partial y}\right)^2+\left(\frac{\partial u_x^2}{\partial x}-\frac{\partial u_y^2}{\partial y}\right)^2 + \left(\frac{\partial u_x^1}{\partial y}+\frac{\partial u_y^1}{\partial x}\right)^2+\left(\frac{\partial u_x^2}{\partial y}+\frac{\partial u_y^2}{\partial x}\right)^2\right] \tag{44}$$

We will split this in two parts. Part A will look at the first square bracket term.

Part A:

$$\begin{aligned}
&\left[\left(\frac{\partial u_x^1}{\partial x}+\frac{\partial u_y^1}{\partial y}\right)^2+\left(\frac{\partial u_x^2}{\partial x}+\frac{\partial u_y^2}{\partial y}\right)^2\right] = \\
&= \left(\frac{\partial u_x^1}{\partial x}\right)^2+\left(\frac{\partial u_y^1}{\partial y}\right)^2+2\left(\frac{\partial u_x^1}{\partial x}\right)\left(\frac{\partial u_y^1}{\partial y}\right)+\left(\frac{\partial u_x^2}{\partial x}\right)^2+\left(\frac{\partial u_y^2}{\partial y}\right)^2+2\left(\frac{\partial u_x^2}{\partial x}\right)\left(\frac{\partial u_y^2}{\partial y}\right) \\
&= \left(\frac{\partial}{\partial x}\left(\frac{u_x^+-u_x^-}{2}\right)\right)^2+\left(\frac{\partial}{\partial y}\left(\frac{u_y^+-u_y^-}{2}\right)\right)^2+2\left(\frac{\partial}{\partial x}\left(\frac{u_x^+-u_x^-}{2}\right)\right)\left(\frac{\partial}{\partial y}\left(\frac{u_y^+-u_y^-}{2}\right)\right) \\
&+\left(\frac{\partial}{\partial x}\left(\frac{u_x^++u_x^-}{2}\right)\right)^2+\left(\frac{\partial}{\partial y}\left(\frac{u_y^++u_y^-}{2}\right)\right)^2+2\left(\frac{\partial}{\partial x}\left(\frac{u_x^++u_x^-}{2}\right)\right)\left(\frac{\partial}{\partial y}\left(\frac{u_y^++u_y^-}{2}\right)\right) \\
&= \frac{1}{2}\left[\left(\frac{\partial u_x^+}{\partial x}\right)^2+\left(\frac{\partial u_x^-}{\partial x}\right)^2+\left(\frac{\partial u_y^+}{\partial y}\right)^2+\left(\frac{\partial u_y^-}{\partial y}\right)^2+2\left(\frac{\partial u_x^+}{\partial x}\right)\left(\frac{\partial u_y^+}{\partial y}\right)+2\left(\frac{\partial u_x^-}{\partial x}\right)\left(\frac{\partial u_y^-}{\partial y}\right)\right] \\
&= \frac{1}{2}\left[\left(\frac{\partial u_x^+}{\partial x}+\frac{\partial u_y^+}{\partial y}\right)^2+\left(\frac{\partial u_x^-}{\partial x}+\frac{\partial u_y^-}{\partial y}\right)^2\right]
\end{aligned} \tag{45}$$

In part B we will look at the second square bracket term.

$$\frac{1}{2}\left[\left(\frac{\partial u_x^1}{\partial x}-\frac{\partial u_y^1}{\partial y}\right)^2+\left(\frac{\partial u_x^2}{\partial x}-\frac{\partial u_y^2}{\partial y}\right)^2+\left(\frac{\partial u_x^1}{\partial y}+\frac{\partial u_y^1}{\partial x}\right)^2+\left(\frac{\partial u_x^2}{\partial y}+\frac{\partial u_y^2}{\partial x}\right)^2\right]=$$

$$=\frac{1}{2}\left[\left(\frac{\partial u_x^1}{\partial x}\right)^2+\left(\frac{\partial u_y^1}{\partial y}\right)^2\right]-\left(\frac{\partial u_x^1}{\partial x}\right)\left(\frac{\partial u_y^1}{\partial y}\right)+\frac{1}{2}\left[\left(\frac{\partial u_x^2}{\partial x}\right)^2+\left(\frac{\partial u_y^2}{\partial y}\right)^2\right]-\left(\frac{\partial u_x^2}{\partial x}\right)\left(\frac{\partial u_y^2}{\partial y}\right)$$
$$+\frac{1}{2}\left[\left(\frac{\partial u_x^1}{\partial y}\right)^2+\left(\frac{\partial u_y^1}{\partial x}\right)^2\right]+\left(\frac{\partial u_x^1}{\partial y}\right)\left(\frac{\partial u_y^1}{\partial x}\right)+\frac{1}{2}\left[\left(\frac{\partial u_x^2}{\partial y}\right)^2+\left(\frac{\partial u_y^2}{\partial x}\right)^2\right]+\left(\frac{\partial u_x^2}{\partial y}\right)\left(\frac{\partial u_y^2}{\partial x}\right)$$

$$=\frac{1}{2}\left[\left(\frac{\partial u_x^1}{\partial x}\right)^2+\left(\frac{\partial u_y^1}{\partial y}\right)^2+\left(\frac{\partial u_x^2}{\partial x}\right)^2+\left(\frac{\partial u_y^2}{\partial y}\right)^2+\left(\frac{\partial u_x^1}{\partial y}\right)^2+\left(\frac{\partial u_y^1}{\partial x}\right)^2+\left(\frac{\partial u_x^2}{\partial y}\right)^2+\left(\frac{\partial u_y^2}{\partial x}\right)^2\right]$$

$$=\frac{1}{4}\left[\left(\frac{\partial u_x^+}{\partial x}\right)^2+\left(\frac{\partial u_x^-}{\partial x}\right)^2+\left(\frac{\partial u_y^+}{\partial y}\right)^2+\left(\frac{\partial u_y^-}{\partial y}\right)^2+\left(\frac{\partial u_x^+}{\partial y}\right)^2+\left(\frac{\partial u_x^-}{\partial y}\right)^2+\left(\frac{\partial u_y^+}{\partial x}\right)^2+\left(\frac{\partial u_y^-}{\partial x}\right)^2\right] \tag{46}$$

We put equation (45) and equation (46) together to get the total elastic potential term.

$$U_{\text{elastic}}=\frac{K_A}{4}\left[\left(\frac{\partial u_x^+}{\partial x}+\frac{\partial u_y^+}{\partial y}\right)^2+\left(\frac{\partial u_x^-}{\partial x}+\frac{\partial u_y^-}{\partial y}\right)^2\right]$$
$$+\frac{\mu}{4}\left[\left(\frac{\partial u_x^+}{\partial x}\right)^2+\left(\frac{\partial u_x^-}{\partial x}\right)^2+\left(\frac{\partial u_y^+}{\partial y}\right)^2+\left(\frac{\partial u_y^-}{\partial y}\right)^2+\left(\frac{\partial u_x^+}{\partial y}\right)^2+\left(\frac{\partial u_x^-}{\partial y}\right)^2+\left(\frac{\partial u_y^+}{\partial x}\right)^2+\left(\frac{\partial u_y^-}{\partial x}\right)^2\right] \tag{47}$$

D. Solving $\boldsymbol{u}_-$ in 2D

This appendix serves to fill the gap between equation (27) and equation (28). We had:

$$\sin(\boldsymbol{G}_j^M \cdot \boldsymbol{r} + \boldsymbol{a}_j^* \cdot \boldsymbol{u}) = \sum_{\boldsymbol{q}} f_{\boldsymbol{q}}^j e^{i\boldsymbol{q}\cdot\boldsymbol{r}} \tag{48}$$

So, for different values for j we have:

$$\begin{aligned}
j = 1 \rightarrow \sum_{\boldsymbol{q}} f_{\boldsymbol{q}}^1 e^{i(xq_x+yq_y)} &= \sin\left[\boldsymbol{G}_{1x}^M x + \boldsymbol{G}_{1y}^M y + 2\pi\frac{u_-^x}{a} - 2\pi\frac{u_-^y}{a\sqrt{3}}\right] \\
j = 2 \rightarrow \sum_{\boldsymbol{q}} f_{\boldsymbol{q}}^2 e^{i(xq_x+yq_y)} &= \sin\left[\boldsymbol{G}_{1x}^M x + \boldsymbol{G}_{2y}^M y + \frac{4\pi u_-^y}{a\sqrt{3}}\right] \\
j = 3 \rightarrow \sum_{\boldsymbol{q}} f_{\boldsymbol{q}}^3 e^{i(xq_x+yq_y)} &= \sin\left[G_{3x}^M x + g_{3y}^M y - \frac{2\pi u_-^x}{a} - \frac{2\pi u_-^y}{a\sqrt{3}}\right]
\end{aligned} \tag{49}$$

The partial derivatives for x and y are shown. These we substituted into equation (24) and equation (25) to get equation (28) and equation (29).

$$\begin{array}{l|l}
\frac{\partial u_-^x}{\partial x} = \sum_{\boldsymbol{q}} iq_x \boldsymbol{u}_-^{q_x} e^{i(xq_x+yq_y)} & \frac{\partial u_-^y}{\partial y} = \sum_{\boldsymbol{q}} iq_y \boldsymbol{u}_-^{q_y} e^{i(xq_x+yq_y)} \\
\frac{\partial^2 u_-^x}{\partial x^2} = -\sum_{\boldsymbol{q}} q_x^2 \boldsymbol{u}_-^{q_x} e^{i(xq_x+yq_y)} & \frac{\partial^2 u_-^y}{\partial y^2} = -\sum_{\boldsymbol{q}} q_y^2 \boldsymbol{u}_-^{q_y} e^{i(xq_x+yq_y)} \\
\frac{\partial^2 u_-^x}{\partial x \partial y} = -\sum_{\boldsymbol{q}} q_x q_y \boldsymbol{u}_-^{q_x} e^{i(xq_x+yq_y)} & \frac{\partial^2 u_-^y}{\partial x \partial y} = -\sum_{\boldsymbol{q}} q_x q_y \boldsymbol{u}_-^{q_y} e^{i(xq_x+yq_y)} \\
\frac{\partial^2 u_-^x}{\partial y^2} = -\sum_{\boldsymbol{q}} q_y^2 \boldsymbol{u}_-^{q_x} e^{i(xq_x+yq_y)} & \frac{\partial^2 u_-^y}{\partial x^2} = -\sum_{\boldsymbol{q}} q_x^2 \boldsymbol{u}_-^{q_y} e^{i(xq_x+yq_y)}
\end{array}$$